Regional variation in ICC distribution, pacemaking activity and neural responses in the longitudinal muscle of the murine stomach

Guizhi Song, G. David, S. Hirst, Kenton M. Sanders and Sean M. Ward

Department of Physiology and Cell Biology, University of Nevada School of Medicine, Reno, NV 89557 USA

Intramuscular interstitial cells of Cajal (ICC-IM) play a critical role in enteric neural regulation of the circular muscle layer in the stomach, but no studies have been performed on the longitudinal layer. Kit immunohistochemistry was used to examine ICC-IM in the longitudinal muscle layer of the murine corpus and antrum, and it revealed marked heterogeneity in the distribution of ICC-IM in longitudinal muscles. In the corpus, ICC-IM were found along the greater curvature near the fundus. ICC-IM decreased in density in the circumferential axis toward the lesser curvature and in the longitudinal axis toward the antrum. ICC-IM were absent from the longitudinal layer of the antrum. Double labelling with markers for specific classes of enteric motor neurones revealed that cholinergic and nitrergic motor neurones formed close contacts with ICC-IM in the corpus but not in the antrum. Enteric nerve stimulation evoked prominent cholinergic excitatory and nitrergic inhibitory responses in longitudinal muscles of the corpus, but not in the antrum of wild-type animals. Cholinergic and nitrergic nerves were also present in W/W^V mice, but functional innervation of the longitudinal muscle layer by these nerves in the corpus and antrum were absent. The data show that cholinergic and nitrergic neurotransmission only occurs in the gastric longitudinal layer in regions where ICC-IM are present. In regions, such as the corpus, where ICC-IM are common, robust neural responses are present, but the reduced density of ICC-IM near the lesser curvature and in the distal stomach leads to reduced neural regulation in these gastric regions.

(Received 10 December 2004; accepted after revision 26 January 2005; first published online 27 January 2005)
Corresponding author S. M. Ward: Department of Physiology and Cell Biology, University of Nevada School of Medicine, Reno, NV 89557 USA. Email: sean@physio.unr.edu

Electrical slow-wave activity in the gastrointestinal tract is generated by specialized cells known as interstitial cells of Cajal (ICC). In phasic regions of the stomach, slow waves are initiated by ICC that form a network in the myenteric region between the circular and longitudinal muscle layers (ICC-MY). Slow waves actively propagate through the ICC-MY network and conduct into adjacent, electrically coupled muscle layers (Ördög *et al.* 1999; Cousins *et al.* 2003). A second population of ICC, referred to as intramuscular ICC (ICC-IM), are intermingled with smooth muscle cells in muscle bundles of the circular and longitudinal muscle layers (Burns *et al.* 1996). These cells are essential for cholinergic and nitrergic neurotransmission in circular muscles of the fundus (Burns *et al.* 1996; Ward *et al.* 2000; Beckett *et al.* 2002) and antrum (Hirst *et al.* 2002*b*; Suzuki *et al.* 2003; Beckett *et al.* 2003). A third population of ICC lie along the surfaces of circular muscle bundles in the connective tissue septae that separate the muscle bundles, and are referred to as ICC-SEP (Ward & Sanders, 1990). ICC-SEP may provide an active propagation pathway for distribution of slow waves from ICC-MY through the muscle layers in larger animals (Horiguchi *et al.* 2001).

Neural information, transmitted via ICC-IM, can influence the behaviour of the pacemaker ICC-MY. Electric field stimulation of enteric nerve processes in small muscle bundles of the guinea pig antrum, which contain only smooth muscle cells and ICC-IM, evoked cholinergic neural responses. When the bundles were attached to the ICC-MY network, vagal nerve stimulation induced premature pacemaker potentials (Hirst *et al.* 2002*b*), and repetitive stimulation paced the muscles (Beckett *et al.* 2003). This type of regulation was absent in W/W^V mice that lack ICC-IM (Beckett *et al.* 2003). Although a role for ICC-SEP cannot be ruled out in these responses (these cells are also lost in W/W^V mice), the findings suggest that neurally activated depolarization of ICC within the muscle layers can initiate premature slow waves in ICC-MY, and

 DOI: 10.1113/jphysiol.2004.081067

repetitive excitatory nerve stimulation may allow ICC-IM to become the dominant pacemaker.

The physiological evidence suggesting that ICC-IM mediate enteric neural responses and modify pacemaker activity has come primarily from studies of circular muscles of the lower oesophageal sphincter and of the gastric fundus, antrum and pyloric sphincter (Ward & Sanders, 2001; Hirst & Ward, 2003). In the fundus, ICC-IM form a parallel lattice of cells interspersed between nerve terminals and smooth muscle cells in both the circular and longitudinal muscle layers (Burns *et al.* 1996). In the mouse antrum, a dense population of ICC-IM is found in the circular muscle layer running parallel to the circular muscle cells, but few, if any, ICC-IM are found in the longitudinal layer (Hirst *et al.* 2002*a*). Antral ICC-IM have short lateral processes that appear to contact neighbouring ICC-IM cells to form a network (Hirst *et al.* 2002*a*). ICC-IM are found in close apposition to enteric nerve terminals and form gap junctions with smooth muscle cells (Horiguchi *et al.* 2003). As described previously, cholinergic and nitrergic neurotransmission is greatly attenuated in gastric and oesophageal muscles of W/W^V mice that lack ICC-IM, suggesting that these cells have a critical role in mediating neurotransmission. These findings have been contested, however, with the suggestion that loss of neural responses in W/W^V mice might be due to chronic weakening of the contractile apparatus of the smooth muscles of these animals and unrelated to the role of ICC-IM (Sivarao *et al.* 2001).

In the present study we have characterized the distribution of ICC-IM in the longitudinal muscle layer of the corpus and antrum of wild-type and W/W^V mice to determine if there are regional variations in the density of these cells around the circumference and along the length of the stomach. Studies were also performed to examine the functional relationship between enteric nerve processes and ICC-IM in the longitudinal layer, and to determine whether ICC-IM play a role in the cholinergic and nitrergic control of longitudinal muscle layer excitability. The study provides evidence that, unlike circular muscle layer, there is considerable variation in the density of ICC-IM and the contacts between these cells and enteric nerves in the longitudinal muscle layer of the corpus and antrum. Finding regions of longitudinal muscle that lacked ICC-IM provided the opportunity to test whether ICC-IM are important mediators of cholinergic and nitrergic neural responses in gastric muscles isolated from identical wild-type animals.

Methods

Animals

C57Bl6 wild-type and W/W^V mutant mice between the ages of 30 and 60 days were used for the described studies. Animals were obtained from the Jackson Laboratory (Bar Harbour, MN, USA). The animals were maintained and the experiments were performed in accordance with the National Institutes of Health Guide for the Care and Use of Laboratory Animals, and the Institutional Animal Use and Care Committee at the University of Nevada approved all procedures used. On days of experiments, mice were anaesthetized with isoflurane (Baxter, Deerfield, IL, USA) prior to cervical dislocation and decapitation.

Morphological studies

Immunohistochemical analysis was performed on strips of corpus and antral muscles of wild-type and W/W^V mutant mice. Whole mount preparations were prepared after removing the mucosa by sharp dissection. The remaining strips of *tunica muscularis* were pinned to the base of a dish filled with Sylgard elastomer (Dow Corning Corp., Midland, MI, USA) with the circular muscle layer facing upward. Tissues were fixed in either acetone (4°C; 10 min) or paraformaldehyde (4% w/v in 0.1 M phosphate buffer (PB) for 20 min at 4°C). Following fixation, preparations were washed for 60 min in phosphate-buffered saline (PBS; 0.01 M, pH 7.4). Incubation of tissues in 1% bovine serum albumin for 1 h at room temperature containing 0.3% Triton X-100 was used to reduce non-specific antibody binding. For examination of ICC, tissues were incubated overnight at 4°C with a rat monoclonal antibody raised against Kit protein (ACK2; 5 μg ml^{-1} in PBS; Gibco-BRL, Gaithersburg, MD, USA). Immunoreactivity was detected using fluorescein-isothiocyanate (FITC)-conjugated secondary antibody (FITC-anti rat; Vector Laboratories, Burlingame, CA, USA; 1:100 in PBS, 1 h, room temperature). Control tissues were prepared in a similar manner, omitting ACK2 from the incubation solution. Alternatively, tissues were prepared for cryostat sections as previously described (Iino *et al.* 2004).

For double labelling, tissues were fixed, washed and preincubated in bovine serum albumin for 1 h (1% in PBS) before being incubated sequentially in a combination of primary antibodies. Tissues were incubated overnight at 4°C in primary antibodies. For double-label immunostaining, the first incubation was carried out for 24 h at 4°C. The tissue was subsequently washed in PBS before being incubated in a second antibody for an additional 24 h at 4°C. The combinations of antibodies used were rat/sheep and rat/goat (Table 1). Following incubation in primary antibodies, tissues were incubated separately in secondary antibodies (FITC and Texas Red (TR)). All secondary antibodies were purchased from Vector Laboratories, and diluted to 1:100 in PBS. Secondary incubations were performed for 1 h at room temperature. Control tissues were prepared by either omitting primary or secondary antibodies from the incubation solutions. All the antisera were diluted with 0.3% Triton X-100 in 0.01 M

Table 1. Details of antibodies used for immunohistochemistry

Combined antibodies	Resource	Mono- or polyclonal antibodies	Host	Dilution
ACK2/anti-NOS	Gibco BRL, Gaithersburg, MD, USA/ Piers Emson, Mol. Sci. Group, Cambridge, UK	Mono/Poly	Rat/sheep	1:200/1:200
ACK2/antivAChT	Gibco-BRL, Gaithersburg, MD,USA/ Chemicon Inc. Temecula, CA, USA	Mono/Poly	Rat/goat	1:200/1:200

ACK2, anti c-Kit; NOS, nitric oxide synthase; vAChT, vesicular acetylcholine transporter.

PBS (pH 7.4). Tissues were examined with a Zeiss LSM 510 Meta confocal microscope (Zeiss, Germany) with an excitation wavelength appropriate for FITC (488 nm) and TR (595 nm). Confocal micrographs are digital composites of Z-series scans of 10–15 optical sections through a depth of 3–40 μm.

Electrophysiological experiments

After animals were killed, stomachs, including approximately 5 mm of oesophagus and 10 mm of duodenum, were removed and placed in Krebs–Ringer bicarbonate solution (KRB). The gastric corpus and antrum were isolated by a surgical incision across the stomach above a distinct transition line in mucosal structure that separates the fundus from the corpus. A second incision was made across the terminal antrum just above the pylorus. The antrum (12 × 6 mm) was opened along the lesser curvature, and gastric contents were washed away with KRB. The antrum was subsequently pinned to the base of a Sylgard silicone elastomer (Dow Corning Corp., Midland, MI, USA) dish and the mucosa was removed by sharp dissection. For separate studies on the corpus (22 × 10 mm) and antrum, the stomach was divided by an incision across the region of the *incisura angularis* (see Fig. 1). The separate regions of the stomach were isolated and placed in a recording chamber with the serosal aspect of the muscle facing upward.

Impalements of cells were made with glass microelectrodes having resistances of 80–120 MΩ. Transmembrane potentials were recorded with a standard electrometer (Intra 767; World Precision Instruments (WPI), Sarasota, FL, USA). The longitudinal muscle layer in stomachs of mice is approximately 10–15 μm thick in the corpus and 5–10 μm thick in the antrum. Thus, it was necessary to identify the muscle layer in which cells were impaled. This was accomplished on a routine basis by including propridium iodide (0.1% w/v in 3 M KCl) in the electrode filling solution. After intracellular recordings were performed, tissues were fixed with paraformaldehyde (4% (w/v) in 0.1 M PB) and examined with a confocal microscope with the appropriate excitation for propridium iodide (535 nm). Data were recorded onto a PC running AxoScope 8.0 data acquisition software (Axon Instruments), and hard copies were printed using Clampfit analysis software (Axon Instruments). All experiments were performed in the presence of nifedipine (1 μM) to reduce contractions and facilitate impalements of cells for extended periods. It has been previously demonstrated that slow waves in the gastric antrum are not affected by nifedipine (Suzuki & Hirst, 1999; Beckett *et al.* 2003). In all experiments, parallel platinum electrodes were placed on either side of the muscle strips, and neural responses were elicited by square wave pulses of electrical field stimulation (EFS; 0.1–0.5 ms pulse durations, one pulse −20 Hz, train duration of 1000 ms, 10–15 V) using a Grass S48 stimulator (Quincy, MA, USA).

Isometric force measurements

Separate mechanical experiments were performed on gastric corpus and antrum using standard organ bath techniques. Muscles were dissected as described for electrophysiological experiments, and the mucosa was removed by sharp dissection. Muscle strips (approximately 4 × 2 mm) were isolated and attached to a fixed mount and to a Fort 10 isometric strain gauge (WPI). The muscles were immersed in organ baths maintained at 37 ± 0.5°C with oxygenated KRB. A resting force of 1.0–2.0 mN was applied, which was shown to set the muscles at optimum length (data not shown). This was followed by an equilibration period of 1 h, during which time the bath was continuously perfused with oxygenated KRB. Neural responses were elicited by square-wave pulses of EFS (0.1–0.5 ms pulse durations, one pulse −20 Hz, train duration 10–30 s, 10–15 V) using a Grass S48 stimulator. Signals were recorded using Biopac (Biopac Systems, Santa Barbara, CA, USA), and analysed using Acknowledge software (Biopac Systems, version 3.5.1).

Solutions and drugs

The bath chambers was constantly perfused with oxygenated KRB of the following composition (mM): NaCl 118.5, KCl 4.5, $MgCl_2$ 1.2, $NaHCO_3$ 23.8, KH_2PO_4 1.2, dextrose 11.0, $CaCl_2$ 2.4. The pH of the KRB was 7.3–7.4 when bubbled with 97% O_2–3% CO_2

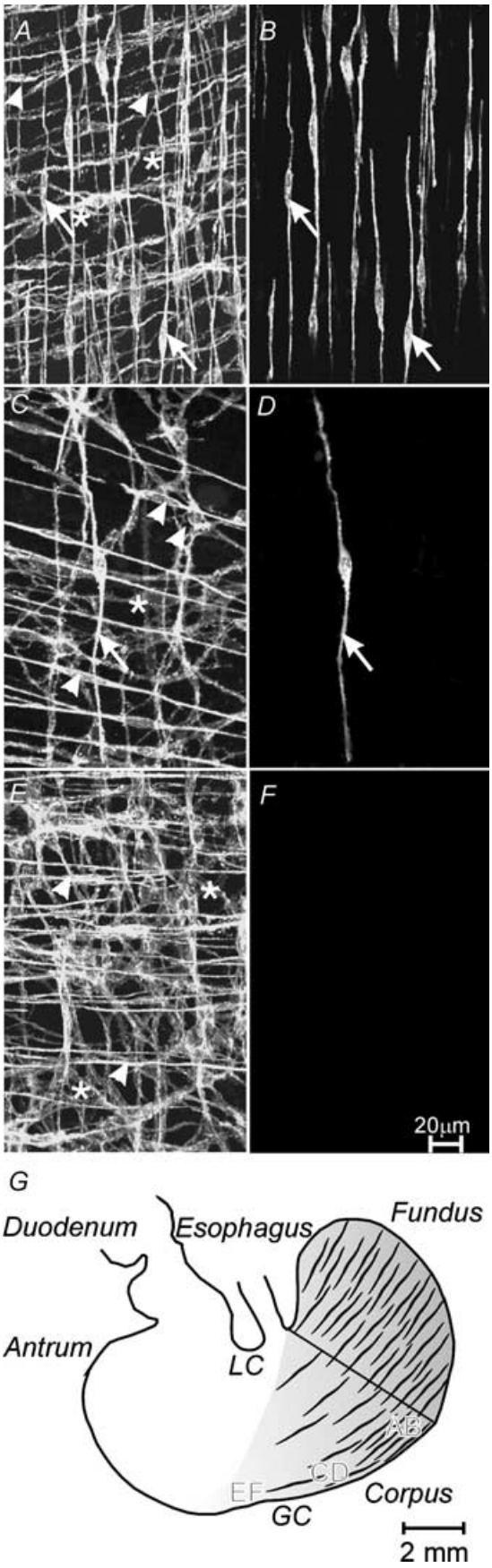

at $37 \pm 0.5^{\circ}$C. Muscles were left to equilibrate for at least 1 h before experiments began. For electrophysiological experiments, nifedipine was obtained from Sigma (St Louis, MO, USA) and dissolved in ethanol at a stock concentration of 10 mM before being added to the perfusion solution at a final concentration of 1 μM. Atropine, apamin, N^{ω}-nitro-L-arginine (L-NA), tetrodotoxin and propridium iodide were also obtained from Sigma, and dissolved in de-ionized H_2O before being diluted in KRB to the final concentration stated in the results section.

Analysis of data

Data are expressed as means $\pm$ standard errors of the mean. Student's *t* test and the Mann–Whitney rank sum test were used where appropriate to evaluate differences in the data. *P* values of less than 0.05 were taken as a statistically significant difference. The '*n*' values reported in the text refer to the number of muscle strips used for each experimental protocol. Each muscle strip used in '*n*' values was taken from a separate animal. Several electrical parameters were analysed: (i) resting membrane potential (RMP), (ii) slow wave amplitude, (iii) duration of slow wave, (iv) inter-slow-wave period, and (v) frequency. Changes in slow-wave duration or inter-slow-wave cycle in response to electrical field stimulation were analysed by averaging the duration of five spontaneous events prior to EFS, and this was compared to the slow wave immediately following EFS. Figures displayed were made from digitized data using Adobe Photoshop 4.0.1 (Adobe Co., Mountain

Figure 1. Distribution of interstitial cells of Cajal (ICC) in the gastric corpus along the greater curvature of the stomach
A and *B*, ICC at a distance of 2 mm from the border between the fundus and corpus (established by the demarcation in the mucosal structure between fundus and corpus; denoted by the line from lesser to greater curvature in *G*). Intramuscular ICC (ICC-IM) were observed within the circular (arrow heads) and longitudinal muscle layers (arrows) and at the level of the myenteric plexus (*). *B*, reconstruction of the longitudinal muscle layer from *A* revealing the density of ICC-IM (arrows). *C* and *D*, the distribution of ICC with the corpus at 5 mm from the fundus–corpus border. ICC-IM within the longitudinal muscle layer (arrow) were significantly decreased in number. *E* and *F*, ICC at a distance of 4 mm from the corpus–antrum border (denoted by the border between shaded and white area and demarcated by the region of the *incisura angularis*). Note that although the numbers of ICC-IM within the circular layer (arrowheads) and ICC-MY (*) were very dense, ICC-IM in the longitudinal muscle layer were absent. *G*, a diagrammatic representation of the density of ICC-IM in the longitudinal layer of the stomach. ICC-IM were present in the fundus and corpus, and were highest in density along the greatest curvature (GC) in the fundus and corpus, and few or absent along the lesser curvature (LC) of the corpus. Images taken in *A–F* are noted on the diagram. The scale bar in *F* is representative for *A–F*. Digital reconstructions were 9 × 1.7, 3 × 1.7, 11 × 1.0, 3 × 1.0, 10 × 1.4 and 3 × 1.4 μm in *A–F*, respectively. Scale bar in *G*, 2 mm.

View, CA, USA) and Corel Draw 7.0 (Corel Corp., Ontario, Canada).

Results

Distribution of ICC in the gastric corpus and antrum

The Kit monoclonal antibody ACK2 was used to examine the regional distribution of ICC in the longitudinal muscle layer of the murine corpus and antrum. Confocal image reconstructions of whole mounts of the gastric corpus revealed ICC at three different locations within the stomach wall. ICC were observed within the circular and longitudinal muscle layers (ICC-IM) running parallel to the long axis of the muscle fibres. ICC were also observed along the intermuscular plane between the circular and longitudinal muscle layers, at the level of the myenteric plexus (ICC-MY; Fig. 1*A*, *C* and *E*). The morphologies of these different populations of ICC were similar to those previously published for the murine stomach (Burns *et al.* 1996; Hirst *et al.* 2002*a*). Examination of the spindle-shaped ICC located within the longitudinal muscle layer revealed a marked heterogeneity in the distribution of these cells along the longitudinal and transverse axes of the corpus (Fig. 1*B*, *D* and *F*). The density of ICC-IM in the longitudinal muscle layer was the greatest close to the border with the fundus (0–2 mm; 5.2 ± 0.2 ICC-IM per random 100 μm transecting line perpendicular to the long axis of the muscle fibres). The density of ICC-IM decreased from the corpus to the antrum (2–4 mm from the border of the fundus, the density was reduced to 2.1 ± 0.4 cells per 100 μm transecting line ($P < 0.01$ compared with 0–2 mm), and 5–6 mm from the fundus the density approached 0 cells per 100 μm transecting line, and 4 mm oral to the *incisura angularis* no ICC-IM were observed in the corpus, $P < 0.01$). Around the stomach, the density of ICC-IM in the corpus was greatest along the greater curvature and decreased towards the lesser curvature of the stomach. Towards the lesser curvature (5 mm from the greater curvature), the density of ICC-IM was 1.8 ± 0.2 cells per 100 μm transecting line compared with 5.2 ± 0.2 ICC-IM along the greater curvature (Fig. 2*A–D*; $P < 0.001$). In W/W^V mutant animals, ICC-IM were absent from the longitudinal and circular muscle layers of the corpus (Fig. 2*G–J*).

Examination of the gastric antrum revealed that although ICC-IM in the circular muscle layer and a dense network of ICC-MY were present in the myenteric plexus region as previously described (Fig. 2*E*; Burns *et al.* 1996; Hirst *et al.* 2002*a*; Beckett *et al.* 2003), ICC-IM were absent from the longitudinal muscle layer in this region of the stomach (Fig. 2*F* and *L*), but not from the circular layer (Fig. 2*K*). In W/W^V mutant animals, ICC-IM were also absent from both longitudinal and circular muscle layers of the antrum (Fig. 2*M* and *N*).

Relationship between enteric nerves and ICC-IM

It has been previously shown that excitatory and inhibitory motor nerves form an intimate relationship with ICC-IM in the circular muscle layer of the gastric fundus and antrum (Ward *et al.* 2000; Beckett *et al.* 2003). To determine if this relationship exists between enteric motor nerves and ICC-IM within the longitudinal muscle layer of corpus and antrum, double-labelling immunohistochemical experiments using antibodies to either vesicular acetylcholine transporter (vAChT) or nitric oxide synthase (nNOS) were performed with an antibody against the Kit receptor.

In the gastric corpus, vAChT-like (vAChT-LI) immunoreactivity revealed a dense network of varicose nerve fibres within the circular and longitudinal muscle layers and in the region of the myenteric plexus (Fig. 3). At a distance of 0–2 mm from the gastric fundus border, there were 6.1 ± 0.3 vACT-LI nerve fibres per 100 μm cross-section transecting line perpendicular to the axis of the longitudinal muscle. At 5 mm from the fundus border, this number had decreased to 1.3 ± 0.14 fibres per 100 μm cross-section transecting line ($P < 0.001$ compared with 0–2 mm). There was also a decrease in the number of vAChT nerve fibres within the longitudinal layer from the greater to lesser curvature. The number of fibres at a distance 0–2 mm from the fundus border decreased from 6.1 ± 0.3 along the greater curvature to 1.7 ± 0.3 fibres per 100 μm transecting line at a distance of 6 mm from the greater to lesser curvature ($P < 0.001$). Double labelling with vAChT and Kit revealed that in the corpus varicose, nerve fibres containing vAChT-LI were closely apposed to ICC-IM (Fig. 3). vAChT nerve fibres were associated with ICC-IM for distances over up to 200 μm. In six animals, 212 ICC-IM were counted; of these, 198 ICC-IM (93.4%) were observed in close association with one vAChT-LI nerve fibre, six ICC-IM (2.8%) were observed with two vAChT nerves, and six ICC-IM (2.8%) did not appear associated with any vAChT-LI immunoreactive nerve fibres, and two ICC-IM (1%) shared one vAChT nerve (Fig. 3).

nNOS-like (nNOS-LI) nerve fibres were also observed in the longitudinal muscle layer for the corpus. At a distance of 0–2 mm from the border of the fundus there were 6.0 ± 0.3 fibres per 100 μm cross-section perpendicular to the axis of the longitudinal muscle along the greater curvature. This number also decreased to 1.3 ± 0.13 fibres at a distance of 5 mm aboral from the fundus border ($P < 0.0001$) along the greater curvature. Similar to vAChT fibres there was a decrease in the number of nNOS-LI nerve fibres from the greater to lesser curvature (6.0 ± 0.3 fibres per 100 μm cross-section along the greater curvature to 1.6 ± 0.2 fibres per 100 μm cross section at a distance of 6 mm from the greater to lesser curvature ($P < 0.0001$)). Double labelling with antibodies against nNOS and Kit also revealed a close apposition between

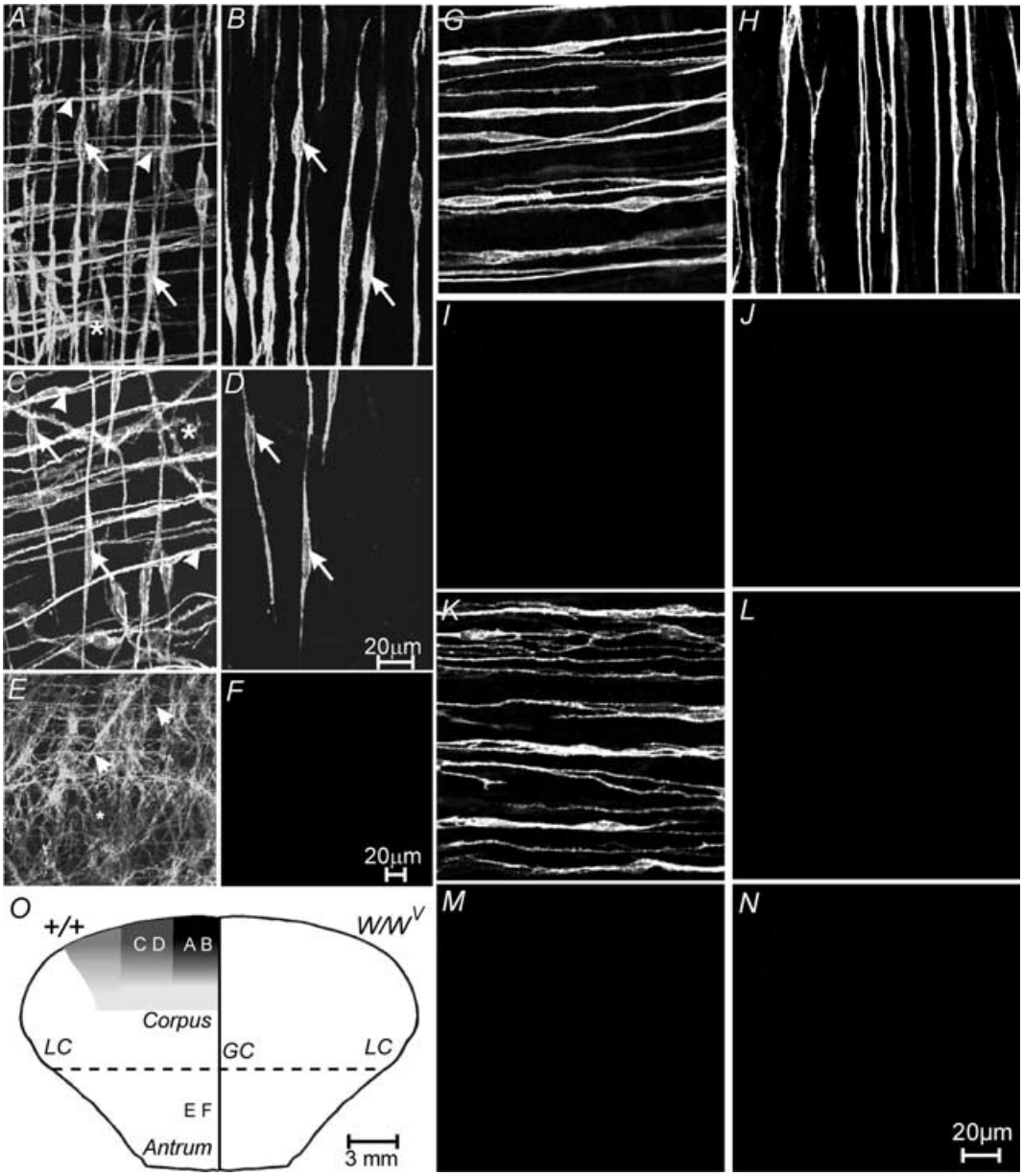

Figure 2. Density of ICC-IM in the gastric corpus and antrum around the stomach in wild-type, and ICC-IM in the corpus and antrum of *W/W^V^* mutants

A, the density of ICC-IM within the circular and longitudinal muscle layers (arrowheads and arrows, respectively) and ICC-MY (*) within the myenteric plexus region at a distance of 2 mm from the greater curvature (GC). *B*, a confocal reconstruction of the longitudinal muscle layer from the same image as shown in *A*, and revealing the density of ICC-IM within the longitudinal muscle layer (arrows). *C*, the reduction in density of ICC-IM and ICC-MY at a distance 6 mm from the greater curvature. *D*, a confocal reconstruction of ICC-IM within the longitudinal layer (arrows) from the image in *C*. Note the drop in density of ICC-IM in the longitudinal layer towards the lesser curvature (LC). *E* and *F*, distribution of ICC in the gastric antrum. *E*, a confocal reconstruction through the entire tunica muscularis. ICC-IM within the circular muscle layer (arrowheads) and ICC-MY at the level of the myenteric plexus can be observed. However ICC-IM within the longitudinal muscle layer are absent. *F*, a confocal reconstruction through the longitudinal muscle layer of the same image confirming the absence of ICC-IM in this layer. *G–N*, ICC-IM in the circular and longitudinal muscle layers of wild-type and *W/W^V^* mutant animals. *G* and *H*, ICC-IM in the circular and longitudinal muscle layers in the corpus of wild-type controls. *I* and *J*, the absence of ICC-IM in the circular and longitudinal layers in the corpus of *W/W^V^* mutants. *K* and *L*, ICC-IM in the circular (*K*) but not the longitudinal layer (*L*) in the antrum of wild-type controls. *M* and *N*, the absence of ICC-IM in the circular and longitudinal layers in the antrum of *W/W^V^* mutant animals. *O*, a diagrammatic reconstruction of the density of ICC in the longitudinal layer of the corpus and antrum of wild-type (+/+, left side) and *W/W^V^* mutant (right side) animals. The greatest density of ICC-IM (black zone on the left labelled from *A* and *B*) was observed

inhibitory motor nerves and ICC-IM in the longitudinal layer. Like vAChT nerve fibres, nNOS nerves were closely apposed to ICC-IM for up to 200 μm. In five animals studied, 225 ICC-IM were counted; of these, 215 ICC-IM (95.6%) were closely associated with one nNOS-positive nerve fibre, three ICC-IM (1.3%) were associated with two nNOS nerve fibres, one ICC was associated with two nNOS nerve fibres, and six ICC-IM were not associated with any nNOS nerve fibre (Fig. 4).

In the gastric antrum, double labelling with vAChT-LI and Kit-LI revealed that there was also a dense network of nerve fibres in the circular and longitudinal muscle

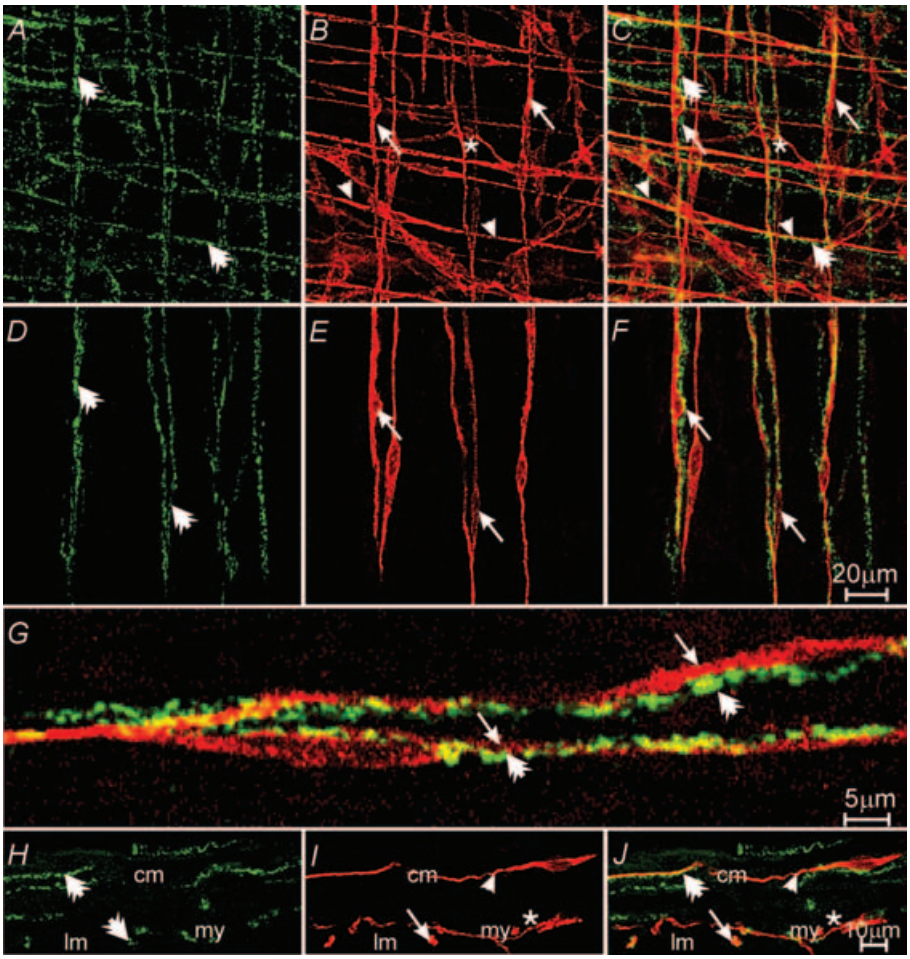

Figure 3. Relationship between excitatory enteric nerves and ICC-IM in the gastric corpus
A, a confocal reconstruction through the myenteric region, including a portion of the circular and longitudinal muscle layers. vesicular acetylcholine transporter (vAChT)-like nerve fibres (green, *A*) are indicated by double arrows. *B*, ICC (red) with the circular (arrow heads) and longitudinal muscle (arrows) layers and at the level of the myenteric plexus (*). *C*, a reconstruction of *A* and *B* showing the relationship between excitatory enteric nerves and ICC-IM in both muscle layers. *D–F*, reconstructions through the longitudinal layer. ICC-IM (double arrows in *A* and *C*) form intimate relationships with ICC-IM in the longitudinal muscle layer (*E* and *F*). *F*, a double label of *D* and *E*. *G*, a high-power image of vAChT nerve fibres (double arrows) and ICC-IM (arrows) within the longitudinal muscle layer taken from *F*. *H–J*, transverse cryostat sections labelled with vAChT and Kit. VAChT-positive nerve fibres (double arrows in panels *H* and *J*) form close contact with ICC-IM in both circular (cm) and longitudinal (lm) muscle layers (arrows in *I* and *J*). ICC-MY (*) are also observed at the level of the myenteric plexus (my). Scale bar in *F* is representative of *A–F*, and scale bar in *J* is representative of *H–J*. Digital reconstructions were *A–C*, 20 × 0.6 μm; *D–F*, 3 × 0.6 μm; *H–J*, 6 × 0.4 μm.

adjacent to the greater curvature (GC), and decreased in density towards the lesser curvature (LC; *C* and D). No ICC-IM were observed in the antrum of +/+ animals or in the corpus and antrum of W/W^V mutants (right hand side of *O*). Scale bar in *D* is representative for panels *A–D*. Scale bar in *F* is representative for *E* and *F*. Digital reconstructions were 20 × 1.3, 4 × 1.3, 10 × 1.1, 3 × 1.0 and 3 × 1.1 μm in *A–D*, and 25 × 0.5 and 4 × 0.5 μm in *E* and *F*, respectively. Scale bar in *N* applies to *G–N*.

layers, and at the level of the myenteric plexus in this region of the stomach (Fig. 5*A* and *C*). No ICC-IM were observed in the longitudinal layer in the antrum (Fig. 5*B* and *D*). The density of vAChT-LI nerve fibres was slightly less in the antrum (4.2 ± 0.12 vAChT-LI nerve fibres per random 100 μm cross section) *versus* that found in the corpus ($P < 0.05$, Fig. 6*B*). There were also slightly fewer nNOS nerve fibres observed running parallel to the longitudinal muscle fibres (4.1 ± 0.1 fibres per random 100 μm cross-section; $P < 0.001$ compared with nNOS-LI fibres in the corpus, Fig. 5*D*).

The presence of ICC-IM and their relationship with enteric nerves in the corpus (Figs 3*H–J* and 4*G–I*) and the absence of ICC-IM but not enteric nerves in the antrum (Fig. 5*E–J*) was also confirmed with cryostat sections.

Although ICC-IM were absent from the longitudinal layer of the corpus and antrum of W/W^V mutants, the number of vAChT-LI and nNOS-LI nerves per 100 μm cross-section transecting line perpendicular to the axis of the longitudinal muscle was similar to that of wild-type animals for all regions (Fig. 6).

Electrical activity of the longitudinal muscle of gastric corpus and antrum

Electrical activity was measured in longitudinal muscles of the corpus using standard intracellular recording techniques. Muscle cells were impaled 2 mm from the border with the fundus along the greater curvature. To confirm that longitudinal cells were impaled, cells were filled with propridium iodide (0.1% w/v) while electrical recordings were made (Fig. 7). Longitudinal muscle cells of the corpus had resting membrane potentials of -46 ± 1.0 mV. Cells impaled in 75% of the muscles had

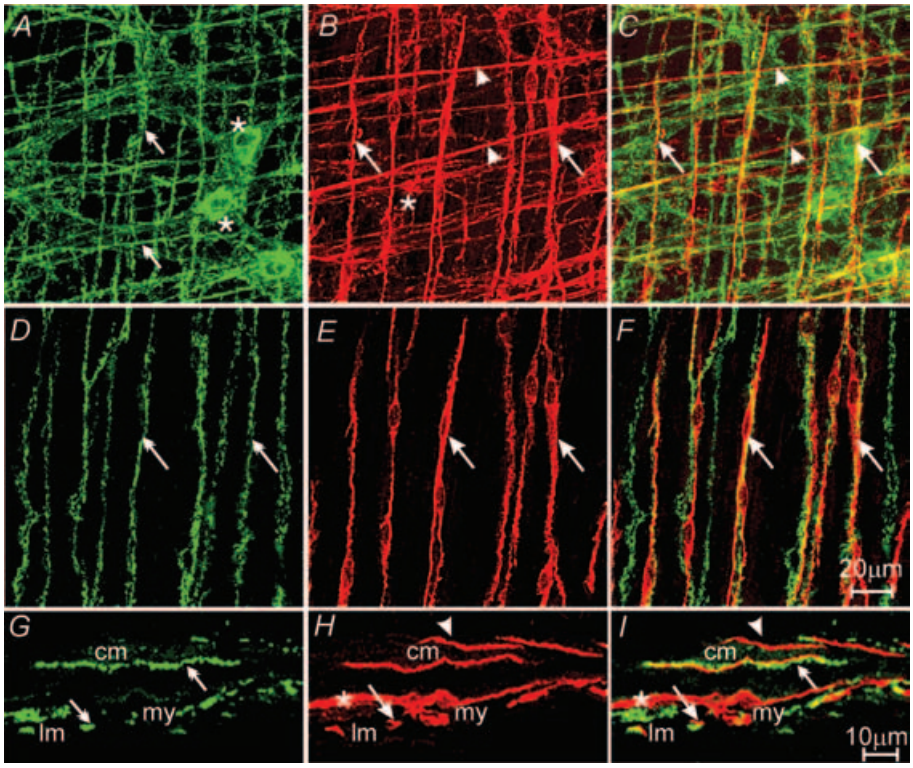

Figure 4. Relationship between inhibitory motor nerves and ICC-IM in the gastric corpus
A, a confocal image reconstruction of nitric-oxide-synthase-like (nNOS-LI) nerve fibres within the circular, and longitudinal muscle layer of the corpus (green, double arrows) and cell bodies within the myenteric plexus region (*). *B*, ICC (red) within the same region of the corpus. ICC-IM in the circular and longitudinal layers, and ICC-MY at the myenteric plexus, are identified with arrowheads, arrows and *, respectively. *C*, double labelling of *A* and *B*, nNOS-LI nerve fibres are closely apposed to ICC-IM within the circular (arrowheads) and longitudinal (arrows) layers. *D–F*, nNOS-LI nerves (green, double arrows) and ICC-IM (red, arrows) within the longitudinal muscle layer. *F*, digital reconstruction of *A* and *B* showing the close apposition between nNOS nerves and ICC-IM (arrows) in the longitudinal layer. *G–I*, confocal images of cryostat sections through the corpus wall. *G*, nNOS-LI nerve fibres (double arrows). *H*, ICC-IM (arrowheads and arrows) and ICC-MY (*). *I*, digital reconstruction of panels *G* and *H*, confirming the close apposition of nNOS-LI and ICC-IM in the circular (arrowheads) and longitudinal muscle (arrows) layers. Scale bar in *F* is representative for panels *A–F*, and scale bar in *I* is representative for panels *G–I*. Digital reconstructions were *A–C*, 25 × 0.5 μm; *D–F*, 3 × 0.5 μm; *G–I*, 3 × 0.6 μm.

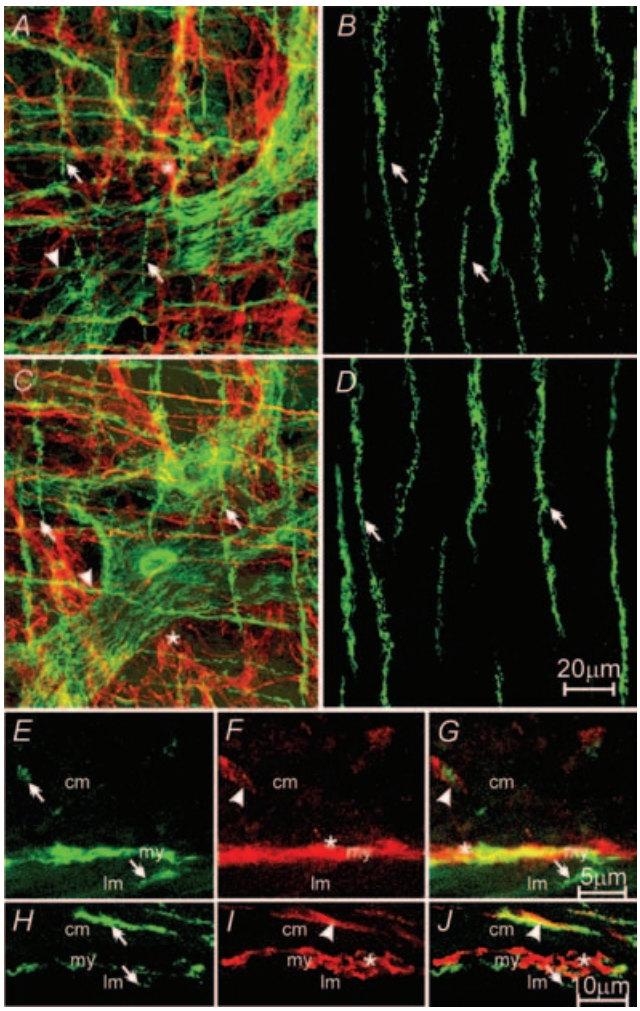

Figure 5. Relationship between excitatory and inhibitory motor nerves and ICC-IM in the longitudinal layer of the gastric antrum
A, a confocal image reconstruction of a double-labelled image of vAChT-LI nerve fibres (green, double arrows) and ICC-IM within the circular (red, arrowhead) and myenteric plexus region (red, *) of the antrum. *B*, a double-labelled image of vAChT-LI and ICC within the longitudinal muscle layer of the same region of antrum. vAChT-LI nerve fibres (double arrows) but no ICC-IM were observed in the longitudinal layer of the antrum. *C* and *D*, a confocal reconstruction of a double-labelled image of nNOS-LI nerves (green, double arrows) and ICC-IM in the circular layer (red, arrowhead), and ICC-MY (red, *) in the myenteric plexus region. *D*, a double-labelled image of nNOS-LI nerve fibres (double arrow) within the longitudinal layer, and an absence of ICC-IM in this layer in the antrum. *E–G*, confocal reconstructions of cryostat sections revealing vAChT-LI nerve fibres (green, double arrows) in the circular (cm) and longitudinal (lm) layers (*E*), and ICC in the circular (ICC-IM, arrowhead) and myenteric plexus (ICC-MY, *) region (my) of the antrum, but not in the longitudinal muscle layer (*F*). Double labelling (*G*) shows vAChT-LI nerves in close apposition to ICC-IM in the circular (arrowhead) but not in the longitudinal layer (double arrow). *H–J*, confocal reconstructions of a transverse cryostat section of the antrum. nNOS-LI nerve fibres (green, double arrows) were observed in the circular (cm) and occasional fibres in the longitudinal (lm) layer. In *I*, ICC (red) were distributed similar to that described for *F*. *J*, a double-labelled image revealing the close apposition between nNOS-LI nerve fibres (double arrows) and ICC-IM (arrowhead) in the circular layer but not in the longitudinal layer of the antrum. Scale bar in *D* is representative for *A–D*. Scale bar in *G* is representative for *E–G*. Scale bar in *J* is representative for panels *H–J*. Digital reconstructions were: *A*, 15 × 1.0 μm; *B*, 4 × 1.0 μm; *C*, 25 × 0.6 μm; *D*, 3 × 0.6 μm; *E–G*, 4 × 0.5 μm; *H–J*, 3 × 0.6 μm.

small irregular membrane potential oscillations ($n = 20$; Fig. 7*C*). Cells in the remaining 25% of muscles had more regular (slow-wave) oscillations with an average amplitude of 3.7 ± 1.0 mV, duration of 2.3 ± 0.1 s, and frequency of 8.9 ± 0.3 cycles min^{-1} (Fig. 7*C*).

Longitudinal smooth muscle cells in the antrum had resting membrane potentials averaging -64.1 ± 1.1 mV. Regular slow waves, 33.3 ± 1.26 mV in amplitude and 7.1 ± 0.1 s in duration, occurred at a frequency of 4.1 ± 0.22 cycles min^{-1}. Intervals between slow waves averaged 7.5 ± 0.4 s ($n = 10$ muscles, Fig. 7*D*). In the corpus we noted considerable noise in recordings of membrane potential (unitary potentials), as previously described in studies of the fundus (see Burns *et al.* 1996; Ward *et al.* 2000; Beckett *et al.* 2002) and antrum (Edwards *et al.* 1999; Suzuki *et al.* 2003). This noisy baseline activity was not apparent in antral longitudinal cells. Slow waves in the antrum also had large square-shaped waveforms similar to those observed from recordings of longitudinal muscle cells in the guinea-pig antrum. These events have previously been referred to as 'follower potentials' to distinguish them from events recorded from circular muscle cells (Dickens *et al.* 1999).

Electrical responses to nerve stimulation

Previous studies have shown that ICC-IM are required for postjunctional responses to cholinergic and nitrergic motor neurones in circular muscles of the gastric fundus and antrum (Burns *et al.* 1996; Ward *et al.* 2000; Beckett *et al.* 2002; Suzuki *et al.* 2003). Here we examined electrical responses to nerve stimulation in longitudinal muscles of the corpus and antrum. EFS (1–20 Hz, 0.1–0.5 ms for 1 s) of corpus muscles evoked biphasic responses. The first phase consisted of a rapid depolarization or excitatory junction potential (EJP) averaging 5.0 ± 0.5, 7.0 ± 0.5, 8.0 ± 1.0 or 9.0 ± 1.5 mV in amplitude, and 0.5 ± 0.02, 0.9 ± 0.1, 0.8 ± 0.1 or 0.7 ± 0.1 s in duration at 1, 5, 10 and 20 Hz, respectively. The EJP was followed by a longer and more pronounced hyperpolarization or inhibitory junction potential (IJP) averaging 5.0 ± 2.0, 8.0 ± 1.0, 9.0 ± 1.0 or 11.0 ± 1.0 mV in amplitude, and 0.8 ± 0.1, 2.0 ± 0.2, 2.5 ± 0.1 or 2.8 ± 0.2 s in duration for 1, 5, 10 and 20 Hz stimuli, respectively ($n = 9$; Fig. 8). Addition of the nitric oxide synthase inhibitor L-NA (100 μM) abolished IJPs at 5–20 Hz, and prolonged the duration of EJPs produced by trains of impulses. In the continued presence of L-NA, atropine (1 μM) abolished the EJPs and unmasked a fast IJP that averaged 7 ± 1.6 mV in amplitude

and 1.45 ± 0.2 s in duration at 20 Hz ($n = 6$). The fast IJP was blocked by apamin (0.2 μM) or tetrodotoxin (1 μM). These data suggest that corpus longitudinal muscles are innervated by both excitatory cholinergic and nitregic/purinergic inhibitory neurones (Mackenzie & Burnstock, 1980).

Neural responses in the antrum differed from those of the corpus. EFS (1–20 Hz, 0.1–0.5 ms duration for 1 s) produced biphasic responses consisting of an IJP followed by phase advancement of the next slow wave after the stimulus. At higher stimulation frequencies (10–20 Hz), membrane potential depolarized and the duration of slow waves was enhanced for the next several slow-wave cycles. For example, the average slow-wave duration increased from 7.1 ± 0.1 s prior to EFS to 9.3 ± 0.7 s (at 10 Hz; $P < 0.05$), and to 16.4 ± 2.2 s (at 20 Hz; $P < 0.005$). At the same time, the inter-slow-wave interval decreased from 7.5 ± 0.4 to 3.01 ± 0.23 s at 10 Hz ($P < 0.001$), and to 2.8 ± 0.29 s at 20 Hz ($P < 0.001$; $n = 10$; Fig. 9).

L-NA (100 μM) did not affect the nature of these responses at lower stimulation frequencies (i.e. 1–10 Hz), but at 20 Hz the depolarization in response to EFS was potentiated, and the duration of slow waves following EFS was increased ($n = 5$; Fig. 9). In the presence of L-NA, atropine (1 μM) did not alter responses of longitudinal muscles to EFS ($n = 5$; Fig. 9). The fast IJP observed under control conditions and in the presence of L-NA was blocked by apamin (0.2 μM; $n = 5$; not shown) and TTX (1 μM; Fig. 9). The increase in duration of the slow waves following EFS was inhibited by TTX (1 μM); however, the phase advancement in slow waves persisted at higher stimulation frequencies (20 Hz; Fig. 9). These data would suggest that the longitudinal muscle layer of the murine antrum receives little or no functional innervation from excitatory cholinergic or inhibitory nitrergic nerves.

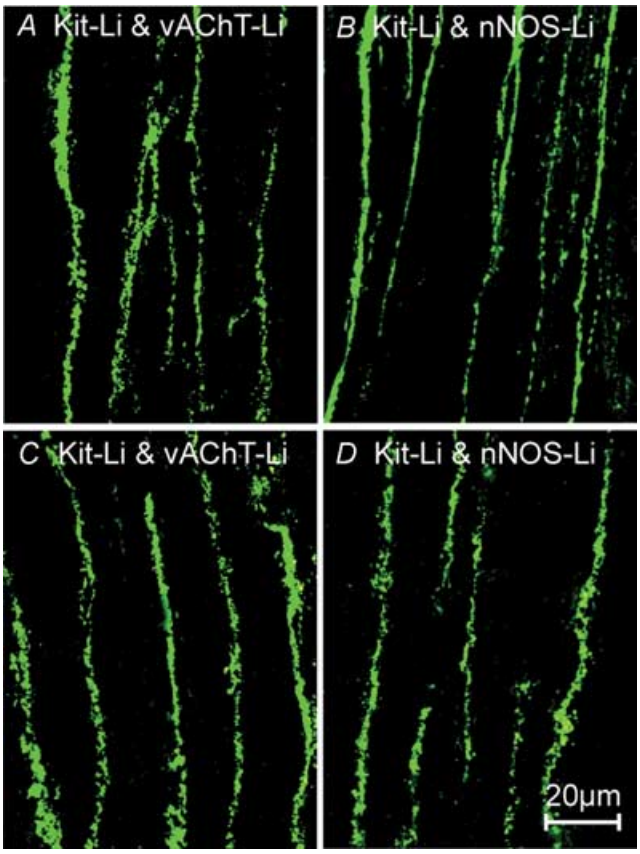

Figure 6. Distribution of vAChT and NOS-like immunoreactive nerves in the corpus and antrum of *W/W^V* mutant animals
A and *B*, vAChT and nNOS-LI immunoreactivity in the corpus, respectively. *C* and *D*, the distribution of vAChT and nNOS-LI nerves in the antrum of *W/W^V* mutant animals. Scale bar in *D* is 20 μm, and is representative for all panels.

Neural responses to EFS in the corpus and antrum of *W/W^V* mutant animals

Muscles of wild-type mice have reduced ICC-IM in the longitudinal muscle layer, as described previously. But the circular muscle within intact muscles contains an abundance of ICC-IM from corpus through the antrum (Burns *et al.* 1996). It is possible that a portion of the responses we noted, particularly in the antrum could have been due to neurally mediated responses via circular muscle ICC-IM. Therefore, we also recorded from muscles of *W/W^V* mice, which lack all ICC-IM in the corpus and antrum. Resting membrane potentials of longitudinal muscle cells of corpus muscles of *W/W^V* mice, recorded 2 mm from the fundus border as in wild-type animals, averaged -48.6 ± 1.3 mV ($n = 5$; Fig. 10), and the recordings lacked the characteristic noisy baseline observed in recordings from wild-type muscles (compare Fig. 7*C* with Fig. 7*E* and Beckett *et al.* 2004). EFS (0.3 ms, 1–20 Hz for 1 s) produced little or no postjunctional responses under control conditions, and responses were not unmasked by addition of L-NA (100 μM), or the combination of L-NA and atropine (1 μM, $n = 5$; Fig. 10*A*–*C*).

Resting membrane potential in cells in the longitudinal muscle of the antrum of *W/W^V* mutants averaged -65.3 ± 0.9 mV, and slow waves of 26.5 ± 3.9 mV in amplitude and 6.0 ± 0.3 s in duration occurred at 4.75 ± 0.25 cycles min^{-1} ($n = 5$; Figs 7*F* and 10*E*–*H*). Stimulation of enteric motor nerves with EFS (0.3 ms, 1–20 Hz for 1 s) initiated IJPs blocked by apamin (0.2 μM). EFS (>5 Hz) caused advancement in the slow wave immediately following the IJP, and at higher frequencies there was a membrane depolarization and an increase in slow-wave frequency for several cycles after EFS (Fig. 10*E*–*H*). L-NA (100 μM; Fig. 10*F*) or L-NA with atropine (1 μM; Fig. 10*G*; $n = 5$) did not effect nerve evoked responses. TTX (1 μM, $n = 5$) abolished all responses to EFS at these parameters (Fig. 10*H*). These responses are essentially the same as responses observed in

wild-type animals, and suggest that longitudinal muscle responses to EFS are not a consequence of stimulation of ICC-IM in the circular layer.

Contractile measurements

We also compared mechanical responses of longitudinal muscles of the corpus and antrum using 2 mm × 4 mm muscle strips prepared from the area along the greater curvature. Spontaneous contractile activity was observed in muscles of both regions. Phasic contractions occurred at $7.5 \pm 0.4\ \text{min}^{-1}$ in the corpus ($n = 11$; Fig. 11) and at $3.4 \pm 0.24\ \text{min}^{-1}$ in the antrum ($n = 15$; Fig. 12). It was difficult to determine the period between contractions in the corpus due to the sinusoidal nature of the contractions. The period between contractions in the antrum was 12.8 ± 2.62 s. Spontaneous contractions in the corpus were weaker than in the antrum (i.e. 0.05 ± 0.01 mN for corpus *versus* $0.45 \pm 0.03\ \text{mN mg}^{-1}$ for antrum; $P < 0.01$). EFS (1–20 Hz, 0.1–0.5 ms duration for 10 s, $n = 7$) caused an initial relaxation of corpus muscles that was followed by contraction. The two phases of the response were frequency dependent (Fig. 11*A*). L-NA (100 μM) blocked the relaxation phase and potentiated the contractile phase (Fig. 11*B*). The contractile event was inhibited by atropine (1 μM; Fig. 11*C*). After L-NA and atropine, high-frequency stimulation (i.e. 20 Hz) yielded small contractions that were blocked by TTX (1 μM; Fig. 11*D*). EFS also evoked frequency-dependent contractions in longitudinal corpus muscles of W/W^V mice. These averaged 0.11 ± 0.01 and 0.16 ± 0.03 mN at 5 and 10 Hz, respectively. L-NA (100 μM) and atropine (1 μM) had little or no effect on contractile responses to EFS. Any responses that were observed were blocked by TTX (1 μM) (Fig. 11*E*–*H*).

Spontaneous phasic contractions were more regular in longitudinal muscles of the antrum than in the

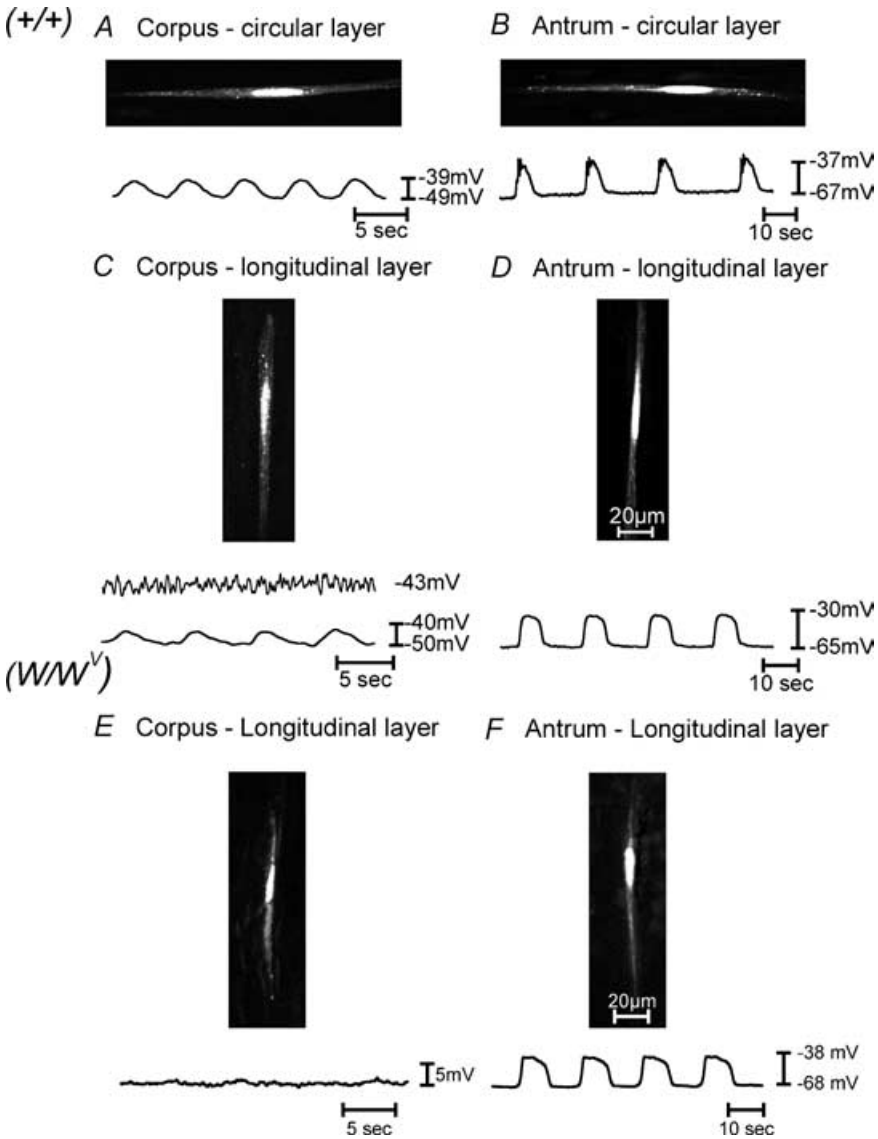

Figure 7. Typical intracellular electrical recordings from the circular and longitudinal muscle layers of the gastric corpus and antrum
A and *B*, slow-wave activity from the circular muscle layer of the corpus and antrum, and *C* and *D*, slow waves from the longitudinal muscle layer of the corpus and antrum of wild-type animals, respectively. *E* and *F*, intracellular recordings from the longitudinal layer of the corpus and antrum of W/W^V mutants. Slow waves from the longitudinal muscle layer of the corpus were typically smaller in amplitude or absent compared with the circular layer of the corpus. Slow waves in the longitudinal layer of the antrum were more rounded in shape and lacked a distinct plateau phase. Note the differences in the membrane noise recorded in the longitudinal layer of the corpus *versus* the antrum of wild-type and W/W^V mutant animals. During recordings, smooth muscle cells were simultaneous filled with propridium iodide (0.1% in 3 M KCl), and images were collected using a Zeiss LSM 510 Meta confocal microscope to verify that the electrical activity was recorded from specific muscle layer.

corpus. EFS (1 Hz, 0.1–0.5 ms duration for 10 s, $n = 7$) produced no significant change in spontaneous activity. However, at 5–20 Hz it caused phase advancement of the contractile event immediately following the stimulus (i.e. period between contractions decreased from 11.5 ± 1.0 s for five cycles before EFS to 3.7 ± 0.6, 2.8 ± 0.6 and 3.3 ± 0.5 s at 5, 10 and 20 Hz, respectively; $P < 0.001$ for all responses; Fig. 12) and a summation of two or more contractions. L-NA (100 μM) caused no change in spontaneous contractile activity or in responses to EFS (Fig. 12*B*). Combination of L-NA and atropine (1 μM) also had no effect on spontaneous or EFS-evoked responses compared with the control (Fig. 12*C*). The phase advancement and summation of contractions following

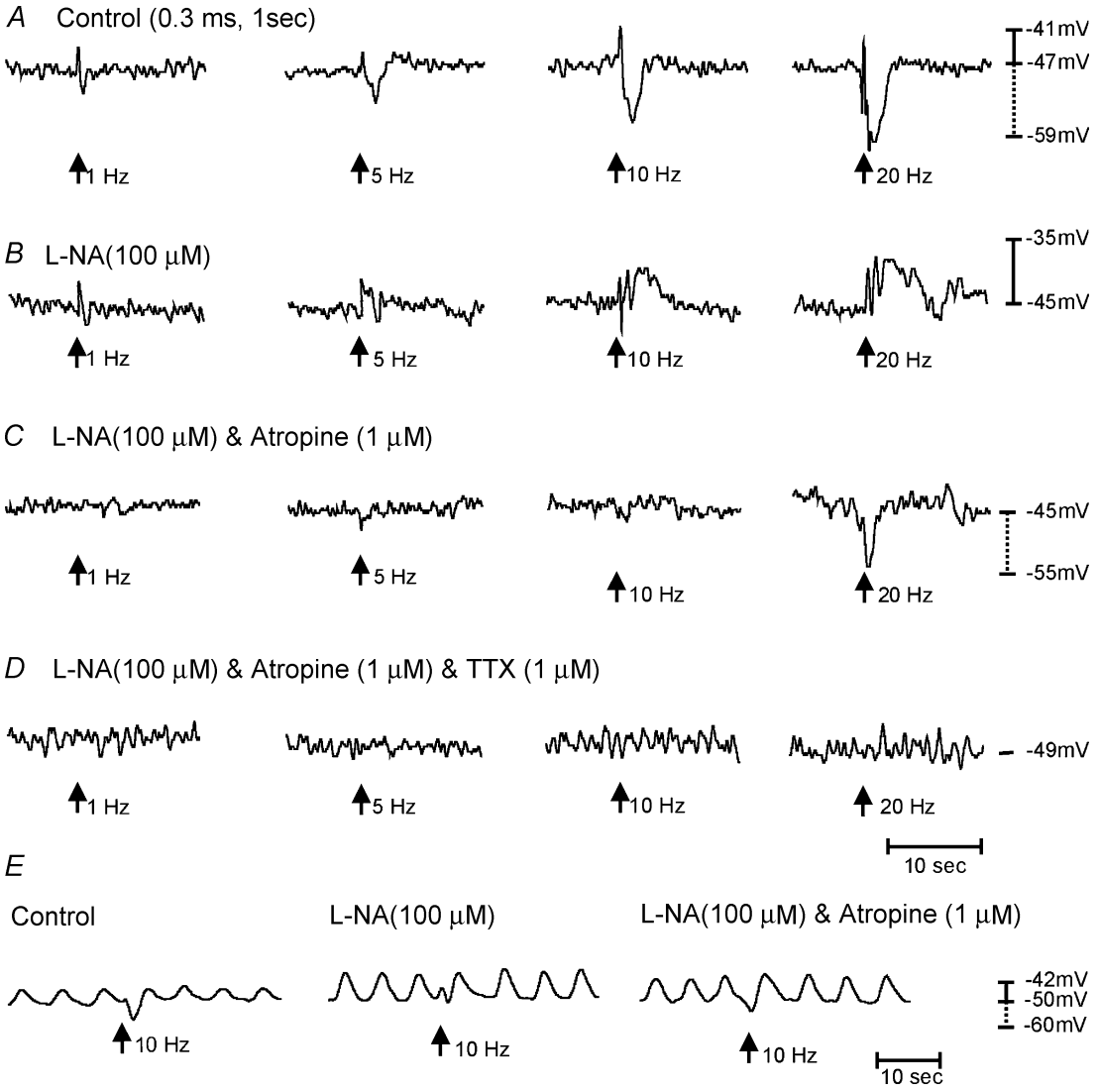

Figure 8. Post-junctional neural responses recorded from the longitudinal muscle layer of the corpus
A, responses to electric field stimulation (EFS) under control conditions. EFS was delivered at arrows (1, 5, 10 and 20 pulses for 1 s; 0.3 ms duration). Excitatory junction potentials (EJPs) and inhibitory junction potential (IJPs) were recorded with all stimulus parameters. IJPs were greater in amplitude and longer in duration at higher stimulus frequencies. *B*, the effects of N^{ω}-nitro-L-arginine (L-NA; 100 μM) to EFS responses. IJPs were blocked by L-NA suggesting that it was mediated by nitric oxide and revealed an underlying depolarization in membrane potential. *C*, the effects of L-NA and atropine (1 μM). The pronounced EJP observed in L-NA was blocked by atropine. EFS at high frequencies (20 Hz) revealed an additional IJP in some tissues with a faster time course than that seen under control conditions. This IJP was blocked by the addition of apamin (0.2 μM) or TTX (1 μM), providing evidence of a neuronal origin for this response (*D*). All recordings were from the same cell. Longitudinal muscle preparations from the corpus occasionally produced slow-wave activity (*E*) Post-junctional neural responses in response to EFS (10 Hz, 0.3 ms pulse duration delivered for 1 s). Immediately after EFS there was a small EJP that was followed by a more pronounced IJP. After L-NA (100 μM), the IJP was blocked and revealed a more pronounced EJP that was sensitive to atropine. After the addition of atropine, an additional IJP was revealed. Recordings in *E* were from the same cell.

EFS was abolished by TTX (1 μM; Fig. 12*D*). In W/W^V mutant animals, EFS caused a similar response to that of wild-type muscles (i.e. phase advancement of the next contraction following stimulation at 5 Hz and greater and a summation of two or more contractions after EFS; Fig. 12*E*). These responses was not affected by L–NA or atropine (Fig. 12*F*–*G*), but were also abolished by TTX (Fig. 12*H*).

These data suggest that a noncholinergic excitatory transmitter is released in sufficient concentrations to excite longitudinal muscles at frequencies of 5 Hz and above. In a further series of contractile experiments, we explored the hypothesis that the noncholinergic neurotransmitter could be a neurokinin. In corpus muscles of wild-type and W/W^V mice, the NK2 antagonist SR-48968 (1 μM) partially inhibited EFS-evoked contractile responses observed after L-NA and atropine. SR-48968 also partially inhibited the phase advancement in slow waves observed in antrum under the same conditions. The NK1 antagonist GR-82334 (1 μM), added in the continued presence of the NK2 antagonist, completely inhibited responses to EFS in the corpus and antrum. These data suggest that higher frequencies of stimulation can release neurokinnins that can directly affect smooth muscle cells or reach the ICC-MY in the antrum (not shown).

Discussion

Morphological and physiological studies have demonstrated the importance of the tight synaptic connections formed by ICC-IM as mediators of excitatory

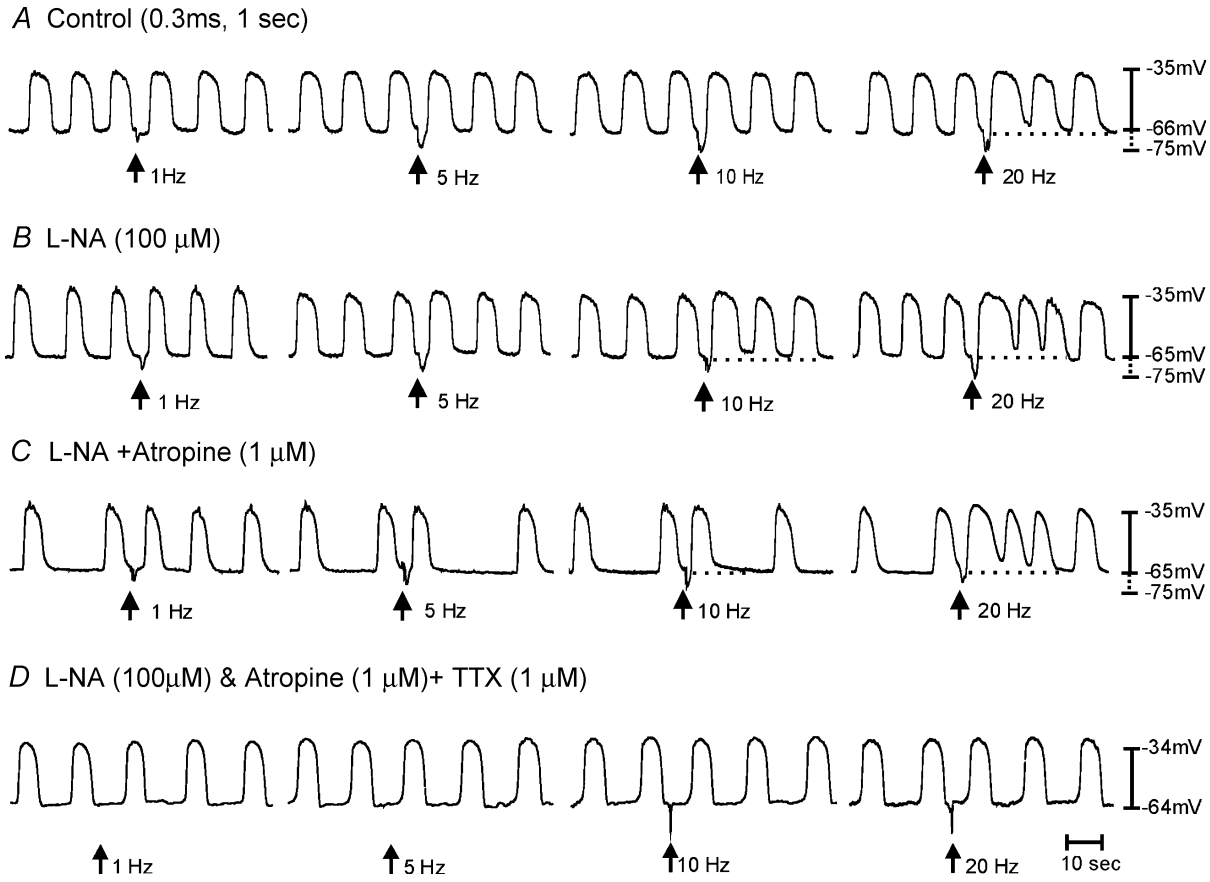

Figure 9. Electrical recordings from the longitudinal muscle layer of the antrum and responses to enteric nerve stimulation

A, typical slow waves and responses to electrical field stimulation under control conditions. EFS (0.3 ms, 1–20 Hz for 1 s; arrows) produced a fast IJP that was evident at all stimulation parameters. At higher frequencies of stimulation (>5 Hz), there was a shortening of the inter-slow-wave period immediately following the IJP, and a prolongation in duration of the slow wave after EFS. At 20 Hz there was also a depolarization in membrane potential for several slow waves following EFS (dashed line). *B*, the lack of effect of L-NA (100 μM) on the fast IJP, the shortening of inter-slow-wave period or the increase in slow wave duration and membrane depolarization (dashed line) after EFS. *C*, in the presence of L-NA, atropine (1 μM) also had no effect on the shortening of the inter-slow-wave period or the increased duration of slow wave and membrane depolarization (dashed line) following EFS, suggesting that cholinergic nerves have little role in the neural activity of the longitudinal layer of the antrum.

and inhibitory enteric motor neurotransmission in the gastric fundus and antrum, and in the lower oesophageal and pyloric sphincters (Burns *et al.* 1996; Ward *et al.* 1998, 2000; Becket *et al.* 2002, 2003; Suzuki *et al.* 2003). Similar morphological relationships exist between enteric motor nerve terminals and ICC-IM in the small intestine (termed ICC-DMP) and colon in a variety of species including man (Thuneberg, 1982; Faussone-Pellegrini, 1987; Rumessen *et al.* 1992, 1993; Torihashi *et al.* 1993; Wang *et al.* 2000, 2003*a*). Functional immunohistochemical studies of these organs, in which activation of second messenger systems linked to specific neurotransmitter pathways have been evaluated, have shown that ICC-IM and ICC-DMP respond to enteric motor neurotransmission (Shuttleworth *et al.* 1993; Wang *et al.* 2003*b*; Iino *et al.* 2004). Physiological evidence to support the role for ICC-IM in neurotransmission has primarily come from studies of gastric circular muscles from W/W^V and Sl/Sl^d mice that lack ICC-IM When ICC-IM are missing, postjunctional excitatory and inhibitory neural responses

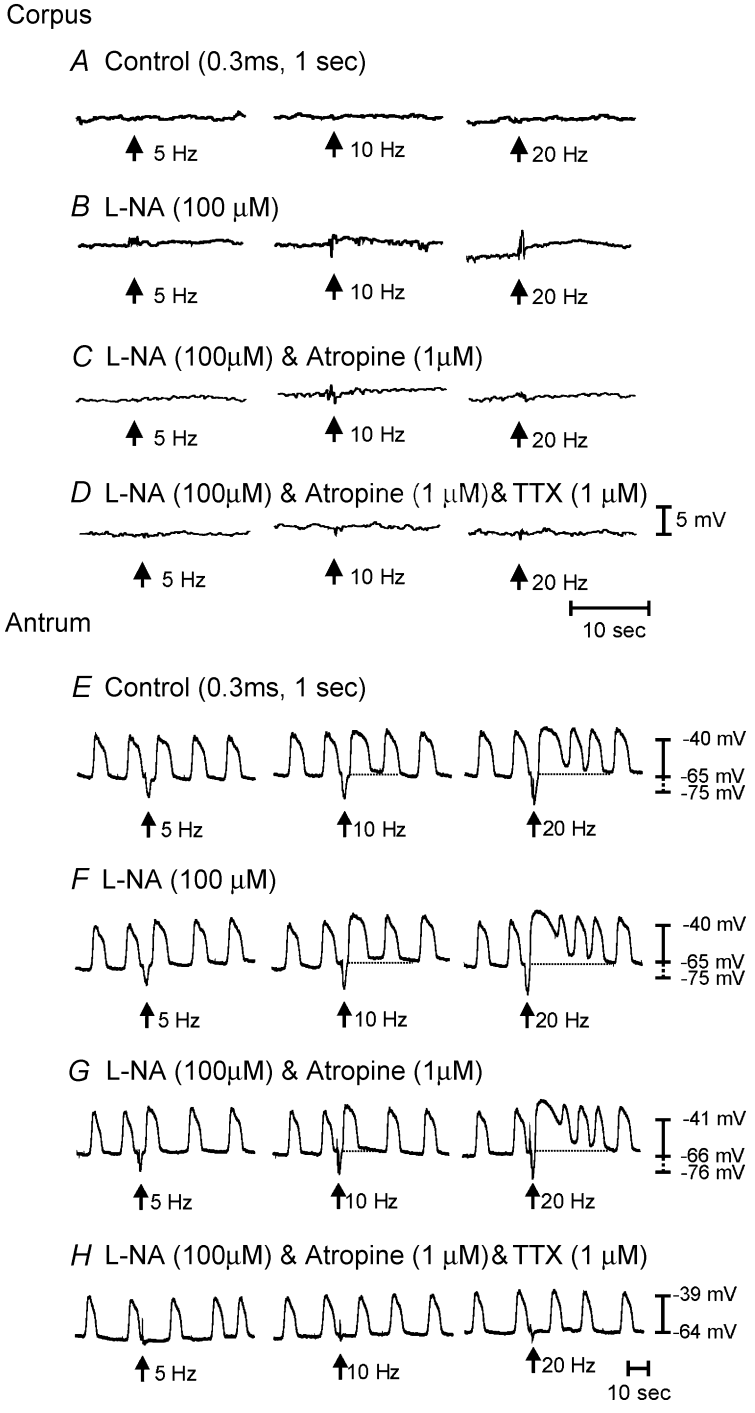

Figure 10. Lack of cholinergic and nitrergic innervation to the longitudinal muscle layer of the corpus and antrum of W/W^V mutant animals
A, lack of response to EFS (0.3 ms, 5–20 Hz for 1 s; arrows) of the corpus under control conditions. *B*, the lack of effect of L-NA (100 μM). *C*, EFS evoked little response in the presence of L-NA and atropine (1 μM), and *D*, TTX (1 μM) also had little effect. *E*, in the antrum under control conditions, EFS (0.3 ms, 5–20 Hz for 1 s, arrows) produced an IJP that was followed by phase advancement and an increase in the duration of the slow wave immediately following EFS. At higher stimulation frequencies (>10 Hz), there was also a depolarization in membrane potential and an increase in slow-wave frequency for several cycles following EFS. *F*, L-NA (100 μM) had no effect on the IJP, phase advancement, membrane depolarization and increase in slow-wave frequency immediately following EFS. *G*, atropine (1 μM) also had no effect on the phase advancement membrane depolarization and increase in slow-wave activity after EFS. However, TTX (1 μM) blocked all nerve-evoked responses except for phase advancement at 20 Hz (*H*).

due to release of acetylcholine and nitric oxide are greatly diminished (Burns *et al.* 1996; Ward *et al.* 1998, 2000; Beckett *et al.* 2003; Suzuki *et al.* 2003). Secondary neural responses, mediated possibly by release of ATP and at higher stimulus frequencies excitatory neurokinins, can be resolved in muscles from W/W^V and Sl/Sl^d mice, suggesting that extrajunctional (i.e. on smooth muscle cells or ICC-MY) receptors may be accessible to noncholinergic/non-nitregic transmitters (Burns *et al.* 1996; Ward *et al.* 1998; Sergeant *et al.* 2002; Beckett *et al.* 2003; Suzuki *et al.* 2003).

The general concept that ICC-IM are required for neurotransmission has been questioned by some investigators who suggested an alternative hypothesis that developmental defects in smooth muscle cells may explain the loss of neural responses in gastrointestinal muscles of W/W^V animals (Sivarao *et al.* 2001). Using intraluminal manometric measurements to examine the lower oesophageal sphincter (LES) pressures, these authors found that the LES of in W/W^V mice was hypotensive, but the sphincter still relaxed in accordance with the swallow reflex or in response to vagal stimulation. It was concluded that the hypotensive nature of the LES was likely to be due to defects in the smooth muscle cells. These authors appear not to have considered an earlier report that responses to exogenous ACh are identical in wild-type and W/W^V muscles (Ward *et al.* 2000), which suggested that smooth muscle function is normal in mutant animals with compromised Kit signalling. This has been confirmed more recently in fundus muscles from Sl/Sl^d animals that also lack ICC-IM (Beckett *et al.* 2002). In the present study we have shown that regions lacking ICC-IM, which occur naturally in wild-type mice, also have reduced nitrergic and cholinergic responses. Our results are consistent with

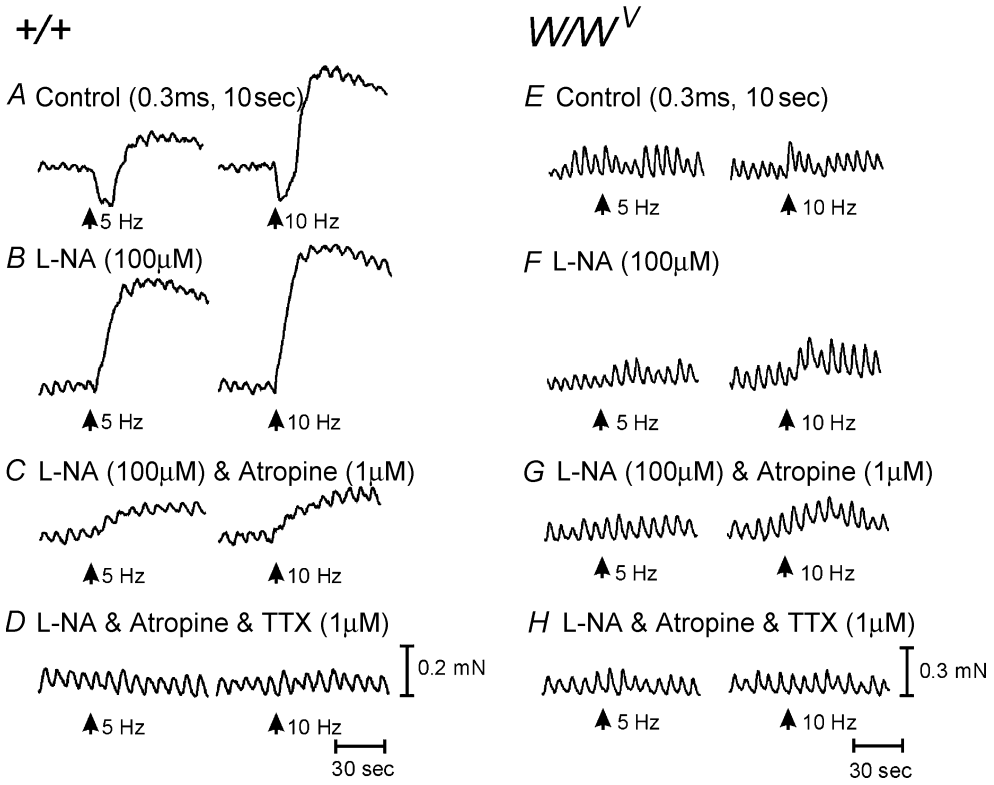

Figure 11. Mechanical activity of the longitudinal muscle layer of the gastric corpus from wild-type and W/W^V mutant animals

A–D, mechanical activity of the longitudinal muscle layer of the gastric corpus of a wild-type animal in response to EFS. *A*, responses to nerve stimulation (0.3 ms, 5 and 10 Hz, for 10 s, arrows) under control conditions. During EFS there was an initial transient relaxation that was followed by a contraction. *B*, the transient relaxation was inhibited by L-NA (100 μM), and a more robust contractile response was observed. *C*, after the addition of atropine (1 μM), a large component of the contraction was inhibited. Any remaining contractions were blocked by the addition of tetrodotoxin (TXX, 1 μM). *E–H*, mechanical activity of the longitudinal muscle layer of the gastric corpus of a W/W^V mutant animal in response to EFS. *E*, responses to nerve stimulation (0.3 ms, 5 and 10 Hz, for 10 s, arrows) under control conditions. EFS produced little or no response at 5 Hz; at 10 Hz or greater there was a small transient contraction. *F*, L-NA (100 μM) had little effect on spontaneous activity or on EFS-evoked nerve activity. *G*, in the presence of L-NA and atropine (1 μM), EFS still evoked transient contractions at frequencies of 10 Hz or greater. *H*, the contractions observed at 10 Hz and greater were inhibited by TTX (1 μM).

the hypothesis that ICC-IM are critical intermediaries in the mediation of postjunctional responses to the primary excitatory and inhibitory neurotransmitters in gastrointestinal muscles.

We examined the distribution of ICC-IM in the in the longitudinal layers of the corpus and antrum, and found a pronounced gradient in the distribution of these cells in which the numbers of ICC-IM rapidly declined in the

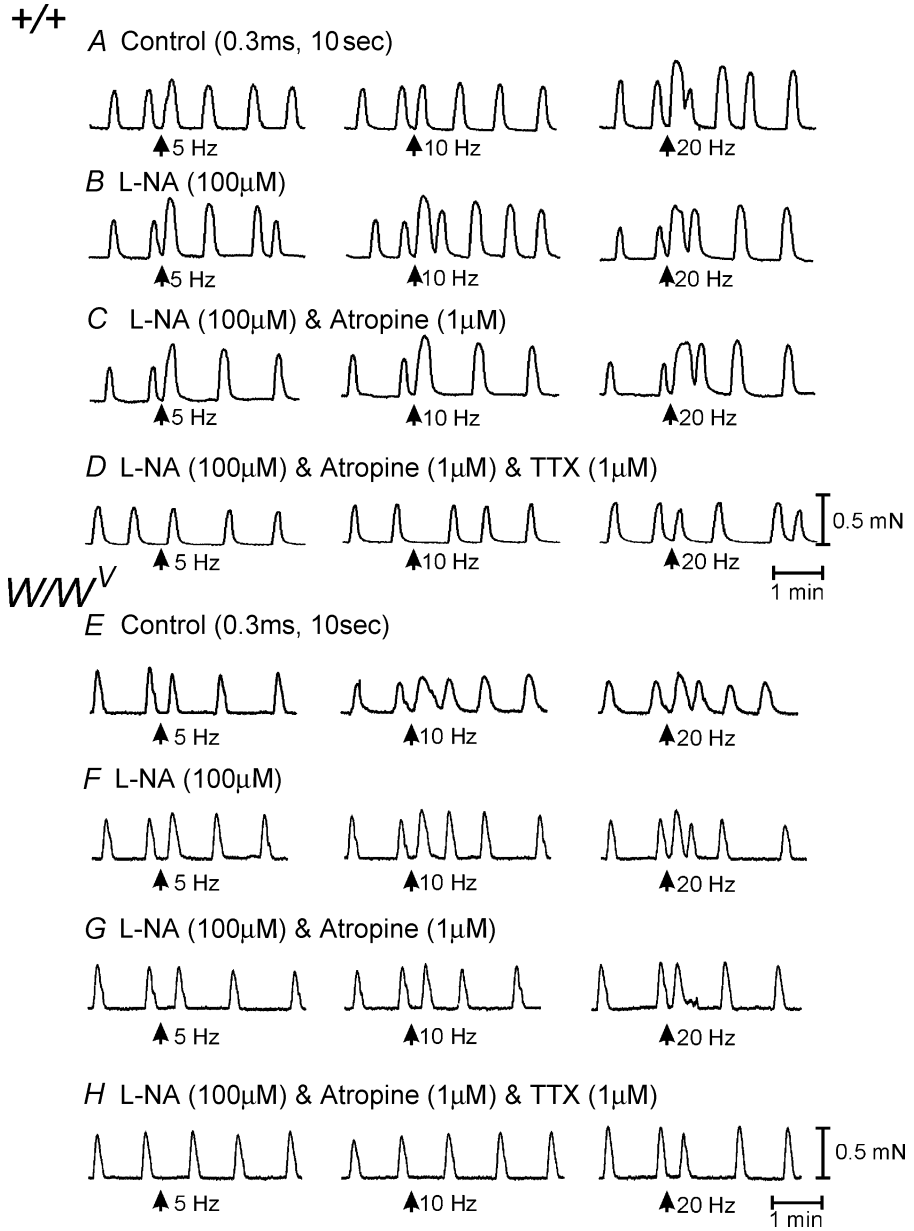

Figure 12. Mechanical activity of the longitudinal muscle layer of the gastric antrum from wild-type and *W/W^V* mutant animals

A–D, mechanical activity of the longitudinal muscle layer of the gastric antrum of a wild-type animal in response to EFS. *A*, responses to nerve stimulation (0.3 ms 5–20 Hz, for 10 s, arrows) under control conditions. During EFS, there was advancement in the phasic contraction immediately following EFS and a slight increase in the amplitude of the phasic contraction. *B*, after the addition of L-NA (100 μM), there was little or no change in the mechanical response to EFS. *C*, atropine (1 μM) also had little or no effect on EFS-induced contractions. *D*, TTX inhibited the increase in phasic contractions to EFS and the advancement in the phasic mechanical activity immediately after EFS (except at 20 Hz). *E–H*, mechanical activity of the longitudinal muscle layer of the gastric antrum of a *W/W^V* mutant animal in response to EFS. *E*, responses to nerve stimulation (0.3 ms 5–20 Hz, for 10 s, arrows) under control conditions. EFS phase advanced mechanical activity at 10 Hz or greater. *F*, L-NA (100 μM) had little effect on spontaneous activity or on EFS-evoked nerve activity. *G*, in the presence L-NA and atropine (1 μM), EFS still evoked a phase advancement of mechanical activity at frequencies of 5 Hz or greater. *H*, the phase advancements in contractions observed at 10 Hz and greater were inhibited by TTX (1 μM).

circumferential axis toward the lesser curvature, and in the longitudinal axis toward the antrum. In the region where ICC-IM were present, robust cholinergic and nitrergic neural responses were recorded. Cholinergic and nitrergic neural responses were not observed in the longitudinal muscle of the antrum that lacked ICC-IM.

The results of this study further emphasize the complexity of neural regulation of the pacemaker mechanism in gastric muscles. It has been previously demonstrated that vagal nerve stimulation in the gastric antrum evokes premature slow waves, and increases the frequency of slow waves. Simultaneous recordings of pacemaker potentials from ICC-MY and slow waves in the circular muscle layer showed that the site of initiation of rhythmical activity switched from ICC-MY to the circular layer, and it was hypothesized that the dominant pacemaker switches from ICC-MY to ICC-IM during vagal stimulation (Hirst *et al.* 2002*b*). Activation of muscarinic receptors of the gastric antrum is capable of increasing the frequency of antral slow waves (Beckett *et al.* 2003). Since this increase in frequency did not occur in the W/W^V mutant mice, it was concluded from this study that the pacing of slow waves by cholinergic neurones occurs via ICC-IM. In the present study, we have observed that at higher frequencies, a noncholinergic neurokinin transmitter can also affect slow-wave frequency, and this can occur in the absence of ICC-IM. Thus, neurokinins, acting via NK1 and NK2 receptors, are capable of affecting pacemaker frequency either by depolarization of smooth muscle cells or by overflow onto nearby ICC-MY.

The fact that neurokinins released from enteric motor neurones can elicit responses in the absence of ICC-IM does not necessarily mean that extrajunctional receptors mediate the effects of neurokinin in wild-type muscles. Several studies have shown that substance-P-containing neurones form very close apposition with ICC-IM in the stomach, and in the deep muscular plexus of the small intestine (Lavin *et al.* 1998; Vannucchi *et al.* 1999; Ibba Manneschi *et al.* 2004; Iino *et al.* 2004). ICC-IM in the small bowel are typically referred to as ICC-DMP, and have similar morphological relationships with enteric motor neurones as ICC-IM in the stomach and colon. NK1 receptor internalization was studied in muscle stimulated with exogenous substance P or with neurokinins released from enteric motor neurones (Iino *et al.* 2004). NK1 receptor internalization occurred in smooth muscle cells and ICC-DMP in response to exogenous substance P, but receptors were internalized only in ICC-DMP in response to neurally released neurokinins (Iino *et al.* 2004). Thus when present, ICC-DMP (ICC-IM) may mediate the majority of neurokinin responses. It is also possible that ICC-IM might express enzymes to metabolize neurokinins released from nerve terminals, and loss of this mechanism could promote escape of neurokinins from the synaptic regions formed by ICC-IM and nerve varicosities to activate nonjunctional receptors.

In summary, there is considerable regional variation in the density of ICC-IM in the longitudinal muscle layer of the corpus and antral regions of the murine stomach. This variation in distribution and density occurs around the greater to lesser curvature and along the stomach wall. Cholinergic and nitrergic neural responses are present when ICC-IM are present in the corpus, but are absent in the antral region of the stomach when ICC-IM are absent. The regional variation in neural responses within the pacemaker region of the stomach could contribute to differences in contractile patterns during mixing of gastric contents.

References

Beckett EA, Bayguinov YR, Sanders KM, Ward SM & Hirst GD (2004). Properties of unitary potentials generated by intramuscular interstitial cells of Cajal in the murine and guinea-pig gastric fundus. *J Physiol* **559**, 259–269.

Beckett EA, Horiguchi K, Khoyi M, Sanders KM & Ward SM (2002). Loss of enteric motor neurotransmission in the gastric fundus of Sl/Sl (d) mice. *J Physiol* **543**, 871–887.

Beckett EA, McGeough CA, Sanders KM & Ward SM (2003). Pacing of interstitial cells of Cajal in the murine gastric antrum: neurally mediated and direct stimulation. *J Physiol* **553**, 545–559.

Burns AJ, Lomax AE, Torihashi S, Sanders KM & Ward SM (1996). Interstitial cells of Cajal mediate inhibitory neurotransmission in the stomach. *Proc Natl Acad Sci U S A* **93**, 12008–12013.

Cousins HM, Edwards FR, Hickey H, Hill CE & Hirst GD (2003). Electrical coupling between the myenteric interstitial cells of Cajal and adjacent muscle layers in the guinea-pig gastric antrum. *J Physiol* **550**, 829–844.

Dickens EJ, Hirst GD & Tomita T (1999). Identification of rhythmically active cells in guinea-pig stomach. *J Physiol* **514**, 515–531.

Edwards FR, Hirst GDS & Suzuki H (1999). Unitary nature of regenerative potentials recorded from circular smooth muscle of guinea-pig antrum. *J Physiol* **519**, 235–250.

Faussone-Pellegrini MS (1987). Comparative study of interstitial cells of Cajal. *Acta Anat (Basel)* **130**, 109–126.

Hirst GD, Beckett EA, Sanders KM & Ward SM (2002*a*). Regional variation in contribution of myenteric and intramuscular interstitial cells of Cajal to generation of slow waves in mouse gastric antrum. *J Physiol* **540**, 1003–1012.

Hirst GD, Dickens EJ & Edwards FR (2002*b*). Pacemaker shift in the gastric antrum of guinea-pigs produced by excitatory vagal stimulation involves intramuscular interstitial cells. *J Physiol* **541**, 917–928.

Hirst GD & Ward SM (2003). Interstitial cells: involvement in rhythmicity and neural control of gut smooth muscle. *J Physiol* **550**, 337–346.

Horiguchi K, Sanders KM & Ward SM (2003). Enteric motor neurons form synaptic-like junctions with interstitial cells of Cajal in the canine gastric antrum. *Cell Tissue Res* **311**, 299–313.

Horiguchi K, Semple GS, Sanders KM & Ward SM (2001). Distribution of pacemaker function through the tunica muscularis of the canine gastric antrum. *J Physiol* **537**, 237–250.

Ibba Manneschi L, Pacini S, Corsani L, Bechi P & Faussone-Pellegrini MS (2004). Interstitial cells of Cajal in the human stomach: distribution and relationship with enteric innervation. *Histol Histopathol* **4**, 1153–1164.

Iino S, Ward SM & Sanders KM (2004). Interstitial cells of Cajal are functionally innervated by excitatory motor neurones in the murine intestine. *J Physiol* **556**, 521–530.

Lavin ST, Southwell BR, Murphy R, Jenkinson KM & Furness JB (1998). Activation of neurokinin 1 receptors on interstitial cells of Cajal of the guinea-pig small intestine by substance P. *Histochem Cell Biol* **110**, 263–271.

Mackenzie I & Burnstock G (1980). Evidence against vasoactive intestinal polypeptide being the non-adrenergic, non-cholinergic inhibitory transmitter released from nerves supplying the smooth muscle of the guinea-pig taenia coli. *Eur J Pharmacol* **67**, 255–264.

Ördög T, Ward SM & Sanders KM (1999). Interstitial cells of Cajal generate electrical slow waves in the murine stomach. *J Physiol* **518**, 257–269.

Rumessen JJ, Mikkelsen HB, Qvortrup K & Thuneberg L (1993). Ultrastructure of interstitial cells of Cajal in circular muscle of human small intestine. *Gastroenterology* **104**, 343–350.

Rumessen JJ, Mikkelsen HB & Thuneberg L (1992). Ultrastructure of interstitial cells of Cajal associated with deep muscular plexus of human small intestine. *Gastroenterology* **102**, 56–68.

Sergeant GP, Large RJ, Beckett EA, McGeough CM, Ward SM & Horowitz B (2002). Microarray comparison of normal and W/W^v mice in the gastric fundus indicates a supersensitive phenotype. *Physiol Genomics* **11**, 1–9.

Shuttleworth CW, Xue C, Ward SM, de Vente J & Sanders KM (1993). Immunohistochemical localization of 3′,5′-cyclic guanosine monophosphate in the canine proximal colon: responses to nitric oxide and electrical stimulation of enteric inhibitory neurons. *Neuroscience* **56**, 513–522.

Sivarao DV, Mashimo HL, Thatte HS & Goyal RK (2001). Lower esophageal sphincter is achalasic in nNOS(–/–) and hypotensive in W/W(v) mutant mice. *Gastroenterology* **121**, 34–42.

Suzuki H & Hirst GD (1999). Regenerative potentials evoked in circular smooth muscle of the antral region of guinea-pig stomach. *J Physiol* **517**, 563–573.

Suzuki H, Ward SM, Bayguinov YR, Edwards FR & Hirst GD (2003). Involvement of intramuscular interstitial cells in nitrergic inhibition in the mouse gastric antrum. *J Physiol* **546**, 751–763.

Thuneberg L (1982). Interstitial cells of Cajal: intestinal pacemaker cells? *Adv Anat Embryol Cell Biol* **71**, 1–130.

Torihashi S, Kobayashi S, Gerthoffer WT & Sanders KM (1993). Interstitial cells in deep muscular plexus of canine small intestine may be specialized smooth muscle cells. *Am J Physiol Gastrointest Liver Physiol* **265**, G638–345.

Vannucchi MG, Corsani L & Faussone-Pellegrini MS (1999). Substance P immunoreactive nerves and interstitial cells of Cajal in the rat and guinea-pig ileum. A histochemical and quantitative study. *Neurosci Lett* **268**, 49–52.

Wang XY, Paterson C & Huizinga JD (2003*a*). Cholinergic and nitrergic innervation of ICC-DMP and ICC-IM in the human small intestine. *Neurogastroenterol Motil* **15**, 531–543.

Wang XY, Sanders KM & Ward SM (2000). Relationship between interstitial cells of Cajal and enteric motor neurons in the murine proximal colon. *Cell Tissue Res* **302**, 331–342.

Wang XY, Ward SM, Gerthoffer WT & Sanders KM (2003*b*). PKC-epsilon translocation in enteric neurons and interstitial cells of Cajal in response to muscarinic stimulation. *Am J Physiol* **285**, G593–G601.

Ward SM, Beckett EA, Wang X, Baker F, Khoyi M & Sanders KM (2000). Interstitial cells of Cajal mediate cholinergic neurotransmission from enteric motor neurons. *J Neurosci* **20**, 1393–1403.

Ward SM, Morris G, Reese L, Wang XY & Sanders KM (1998). Interstitial cells of Cajal mediate enteric inhibitory neurotransmission in the lower esophageal and pyloric sphincters. *Gastroenterology* **115**, 314–329.

Ward SM & Sanders KM (1990). Pacemaker activity in septal structures of canine colonic circular muscle. *Am J Physiol Gastrointest Liver Physiol* **259**, G264–273.

Ward SM & Sanders KM (2001). Interstitial cells of Cajal: primary targets of enteric motor innervation. *Anat Rec* **262**, 125–135.

Acknowledgements

This work was supported by NIH DK57236. The Morphology Core Laboratory, supported by Program Project Grant NIH P01 DK41315, and an equipment grant from the NCRR for the Zeiss LSM510 confocal microscope (1 S10 RR16871), was used for the immunohistochemical studies.